Annual Report of U.S. Airforce Sponsered Project
FA4869-06-01-0065 AOARD 064071

A CO_2 laser rapid-thermal-annealing SiO_x based metal-oxide-semiconductor light emitting diode

Gong-Ru Lin

[2]Graduate Institute of Electro-Optical Engineering
National Taiwan University
1, Roosevelt Rd. Sec. 4, Taipei 106, Taiwan, Republic of China
E-mail: grlin@ntu.edu.tw

Abstract

Structural damage enhanced near-infrared electroluminescence (EL) of a metal-oxide-semiconductor light emitting diode (MOSLED) made on SiO_x film with buried nanocrystallite Si after CO_2 laser rapid-thermal-annealing (RTA) at an optimized intensity of 6 kW/cm^2 for 1 ms is demonstrated. CO_2 laser RTA induced oxygen-related defects are capable of improving Fowler-Nordheim tunneling mechanism of carriers at metal/SiO_x interface. The CO_2 laser RTA SiO_x film reduces Fowler-Nordheim tunneling threshold to 1.8 MV/cm, facilitating an enhanced EL power of an ITO/ SiO_x/p-Si/Al MOSLED up to 50 nW at a current density of 2.3 mA/cm^2.

Index Terms— CO2 Laser annealing, Si nanocrystal, SiOx, Nanotechnology, micro-photoluminescence.

Report Documentation Page

Form Approved
OMB No. 0704-0188

1. REPORT DATE	2. REPORT TYPE	3. DATES COVERED
05 DEC 2007	**Final**	**26-05-2006 to 13-09-2007**

4. TITLE AND SUBTITLE
A Nanocrystallite Si based Metal-Semiconductor-Metal Photosensors and Solar Energy Transformers with Enhanced Responsivity at UV-blue Wavelengths

5a. CONTRACT NUMBER
FA48690610065

5b. GRANT NUMBER

5c. PROGRAM ELEMENT NUMBER

6. AUTHOR(S)
Gong-Ru Lin

5d. PROJECT NUMBER

5e. TASK NUMBER

5f. WORK UNIT NUMBER

7. PERFORMING ORGANIZATION NAME(S) AND ADDRESS(ES)
National Chiao-Tung University,1001 Ta-Hsieh Rd,Hsinchu 300,Taiwan,TW,N/A

8. PERFORMING ORGANIZATION REPORT NUMBER
N/A

9. SPONSORING/MONITORING AGENCY NAME(S) AND ADDRESS(ES)
AOARD, UNIT 45002, APO, AP, 96337-5002

10. SPONSOR/MONITOR'S ACRONYM(S)
AOARD-064071

11. SPONSOR/MONITOR'S REPORT NUMBER(S)

12. DISTRIBUTION/AVAILABILITY STATEMENT
Approved for public release; distribution unlimited

13. SUPPLEMENTARY NOTES

14. ABSTRACT
Structural damage enhanced near-infrared electroluminescence (EL) of a metal-oxide-semiconductor light emitting diode (MOSLED) made on SiOx film with buried nanocrystallite Si after CO2 laser rapid-thermal-annealing (RTA) at an optimized intensity of 6 kW/cm2 for 1 ms is demonstrated. CO2 laser RTA induced oxygen-related defects are capable of improving Fowler-Nordheim tunneling mechanism of carriers at metal/SiOx interface. The CO2 laser RTA SiOx film reduces Fowler-Nordheim tunneling threshold to 1.8 MV/cm, facilitating an enhanced EL power of an ITO/ SiOx/p-Si/Al MOSLED up to 50 nW at a current density of 2.3 mA/cm2

15. SUBJECT TERMS

16. SECURITY CLASSIFICATION OF:			17. LIMITATION OF ABSTRACT	18. NUMBER OF PAGES	19a. NAME OF RESPONSIBLE PERSON
a. REPORT	b. ABSTRACT	c. THIS PAGE			
unclassified	**unclassified**	**unclassified**	**Same as Report (SAR)**	**18**	

I. Introduction

Typically, the synthesis of Si nanocrystals (nc-Si) embedded in plasma enhanced chemical vapor deposition (PECVD)-grown silicon-rich silicon dioxide (SiO_x, x<2) film for efficient light emission requires a long-term and high-temperature furnace-annealing process (longer than 30 min).[1-7] This approach meets the difficulty in its compatibility with current integrated-circuits (ICs) processing limit at temperature <600^oC. Furthermore, conventional annealing methods are not possible to *in-situ* anneal a prescribed area on the SiO_x film with μm scale. CO_2 laser based zone annealing (or zone drawing) technique has previously emerged to modify the morphology or structural properties of different materials including polymers, metallic thin films, and superconductors, and dielectrics etc. Particularly, such a laser heating process was also found to initiate the re-crystallization and sintering of ceramic powders, or to enhance the surface crystallinity and the specific phase of an optical nonlinear crystal (beta-BBO). Optical microscopy has shown that the crystallite surface exhibits same morphology as those observed after traditional furnace processing, however, the effect of CO_2 laser annealing on the growth rate and the crystallite size is more pronounced. Not long ago, the CO_2 laser annealing was primarily employed to improve the properties of a liquid-phase deposited, fluorinated silicon oxide film, which helps to concentrate the fluorinated silicon oxide film and reduce the effective surface charge density caused by surface defect states. Nonetheless, the CO_2 laser annealing induced modifications are intensity (P_{laser}) dependent and usually becomes prominent at Plaser >10 kW/cm^2. Recently, the high-temperature (>1000^oC) furnace annealing is employed to precipitate the Si nanocrystals in SiO_2 film. However, such a high-temperature heat treatment could seriously damages the whole integrated circuits (ICs) on the same Si wafer, which constrains the monolithic integration of the Si nanocrystal doped SiOx layer with the Si based ICs. Owing to the large absorption coefficient as high as 1.2×10^3 cm^{-1} of the oxide material at wavelength of 10.6 μm, a CO_2 laser annealing of SiO_x film on quartz substrate is investigated for the first time. In our previous research, the premier demonstration on synthesizing nc-Si in the SiO_x film by CO_2 laser rapid thermal annealing (RTA) process has been reported to overcome the aforementioned problems.[8,9] Later on, Tewary *et al.*[10] have also demonstrated the locally synthesize light emitting defects and Si nanoparticles in silicon rich oxynitride thin films by using a focused CO_2 laser beam with power densities in the range from 0 to 580 W/cm^2 and times of 5 s to 60 min. Nonetheless, the CO_2 laser annealing SiO_x based light emitting diode has yet not been realized. In this work, we present the fabrication and the

structural/electrical/optical characterization of a metal-oxide-semiconductor light emitting diode (MOSLED), whose oxide layer is the nc-Si embedded SiO_x film fabricated using a CO_2 laser RTA process. The carrier-transport mechanisms and the electroluminescent (EL) properties of such devices are explored in detail.

II. Experimental

PECVD-grown SiO_x film was deposited on the p-type (100) Si substrate with a gas mixture of SiH_4 and N_2O. The process temperature, fluence ratio of SiH_4 to N_2O, the rf power, and the reaction gas pressure were 350^{o}C, 1:6, 40 W, and 60 mtorr, respectively. The thickness of PECVD-grown SiO_x film was 280±10 nm measured by a surface profiler (KLA-Tencor, Alpha-Step 500). Afterwards, the CO_2 laser RTA was performed in atmosphere using a continuous-wave CO_2 laser with ranging from 1.5 to 13.5 kW/cm^2. The laser spot was focused within 0.2 mm using a hemispherical lens. The CO_2 laser illuminating time was as short as 1 ms. The photoluminescence (PL) of CO_2 laser RTA SiO_x pumped by a HeCd laser at 5 W/cm^2 and 325 nm was detected by a fluorescence spectrophotometer (Jobin Yvon, TRIAX-320). Indium tin oxide (ITO) and aluminum (Al) films with thicknesses of 200 nm and 500 nm were used as surface contact and backside contact, respectively. An ITO/$SiO_{1.25}$:nc-Si/p-Si/Al MOSLED with a contact diameter of 0.8 mm was made to perform EL. Rutherford back-scattering (RBS) analysis at a detecting angle of 170^o under 2 MeV He^+-ion bombardment and a commercial software of "RAMP" reveals clear Si and O signals at energies of 1.147 MeV and 742.0 keV, respectively. The calculated O/Si ratio of 1.25 corresponds to a total Si concentration of 44.44 atomic%.

The 280-nm thick SiO_x films were deposited on both-side polished quartz substrates by using high-density plasma enhanced chemical vapor deposition (PECVD) with a gas mixture of SiH_4 and N_2O. The substrate-temperature was kept at 150 ^{o}C for 15 min to balance the temperature of the quartz substrate before deposition. The fluence ratio of SiH_4 to N_2O, the rf power and the reaction gas pressure were 1:6, 50 W and 120 mTorr, respectively. Afterwards, the CO_2 laser RTA was performed in atmosphere using a CW CO_2 laser (LTT Corp., ILS-II with a maximum power of 30 W) with P_{laser} ranging from 1.5 to 13.5 kW/cm^2. The laser spot was focused within 0.2 mm^2 using a hemispherical lens. The CO_2 laser illuminating time was as short as 1 ms. The ablation thickness of SiO_x film was measured by α-step with a resolution of 1 nm. The μ-PL (or μ-PR) of CO_2 laser RTA SiO_x pumped by

a HeCd laser at 5 W/cm^2 and 325 nm was detected by a fluorescence spectrophotometer (Jobin Yvon, TRIAX-320). The μ-PR analysis is demonstrated using a similar system with a HeNe laser at wavelength and power of 632.8 nm and 2 mW, respectively. A HRTEM (JEOL, 4000EX TEM) with a point-to-point resolution of 0.17 nm was used to characterize the orientation, lattice constant, size and density of the precipitated Si nanocrystals in SiO_x film.

III. Results and Discussions

III-1. Surface Temperature Evaluation

During CO_2 laser annealing, the temperature $T(r, z)$ of the annealed $SiO_{1.25}$ film is expressed by the following equation:[11]

$$T(r,z) = \frac{4(1-R)}{\rho C_p} \times \frac{P_{laser}\ \tau}{\pi D^2 d_{absorb}} \times \exp(\frac{-4r^2}{D^2}) \times \exp(-\alpha |z|), \quad (1)$$

where r, z, τ, ρ and C_p are the radial distance, the depth, the illuminating time, the density and the specific heat of the SiO_x film, respectively.[8] P_{laser} is the illuminating intensity of the CO_2 laser, R is the optical reflectivity of $R=[(n-1)^2+k^2]/[(n+1)^2+k^2]$, r is the distance to the center of the focused laser spot, D is the beam diameter at 1/e intensity of the Gaussian distribution, α is the optical absorption coefficient of the SiO_x film, ($\alpha= 4\pi k/\lambda$), λ is the laser wavelength, d_{absorb} is the penetrating depth of the CO_2 laser. The real (n) and imaginary (k) parts of the refractive index of the SiO_x film at the wavelength of 10.6 μm in the room temperature are approximately 2.224 and 0.102, respectively. The optical absorption coefficient (α), the optical reflectivity (R), the Gaussian beam diameter at 1/e intensity (D), the radial distance (r), the illumination time (τ), the density (ρ), and the specific heat (C_p) of the SiO_x film are set as 1209 cm^{-1}, 0.145, 370 μm, 21 μm, 1 ms, 2800 kg/m^3 and 1270 J/kg/K, respectively. According to these parameters, the simulated $T_{surface}$ of the SiO_x film can be increasing from 130 ^{o}C and 3350 ^{o}C as the CO_2 laser P_{laser} enlarges from 1.5 to 13.5 kW/cm^2. Therefore, the $T_{surface}$ of the SiO_x film proportional to the CO_2 laser P_{laser} is estimated from Eq. (2). For example, the SiO_x surface temperature profile around the annealed zone under illuminating with the P_{laser} of 6 kW/cm^2 at the central part of a Gaussian-beam illuminated zone is about 1349^{o}C. Within an illuminating spot of 400μm diameter, the maximum temperature gradient is only 4.5 ^{o}C/μm.

III-2. HRTEM and PL Analysis

After CO_2 laser annealing at laser intensity (P_{laser}) of 6 kW/cm^2 and furnace annealing at 1100^{o}C for 30 min, broadband near-infrared PL spectra with peak wavelengths of 810 nm and 760 nm as well as spectral linewidths of 106 nm and 135 nm are observed (see Fig. 1(a) and 1(b)), respectively, which are attributed to the emission of nc-Si embedded in $SiO_{1.25}$. The estimated surface-temperature of the $SiO_{1.25}$ film at P_{laser} of 6 kW/cm^2 was about 1350^{o}C.[9] The average size of nc-Si buried in CO_2 laser annealed $SiO_{1.25}$ is larger than that of furnace-annealed $SiO_{1.25}$, which contributes the decreasing bandgap of nc-Si and the redshift of PL peak wavelength from 760 to 810 nm.[12] The existence and the size distribution of nc-Si embedded in $SiO_{1.25}$ film annealed at P_{laser} of 6 kW/cm^2 are confirmed by cross-sectional high resolution transmission electron microscopy (HRTEM) images. HRTEM images reveal that the average diameter of nc-Si is about 5.3 nm. The volume density of nc-Si buried in CO_2 laser annealed $SiO_{1.25}$ film is around 1.9 10^{18} cm^{-3}. Another significant PL at 400-650 nm from the CO_2 laser-annealed sample is attributed to incomplete Si precipitation and slight damage of oxide matrix under CO_2 laser annealing within 1ms.[2,3] Such a phenomenon has never been observed in the furnace-annealed sample since the high-temperature and long-term furnace annealing usually causes a gradual recovery on the compressing strain of the SiO_2 matrix nearby the nc-Si.

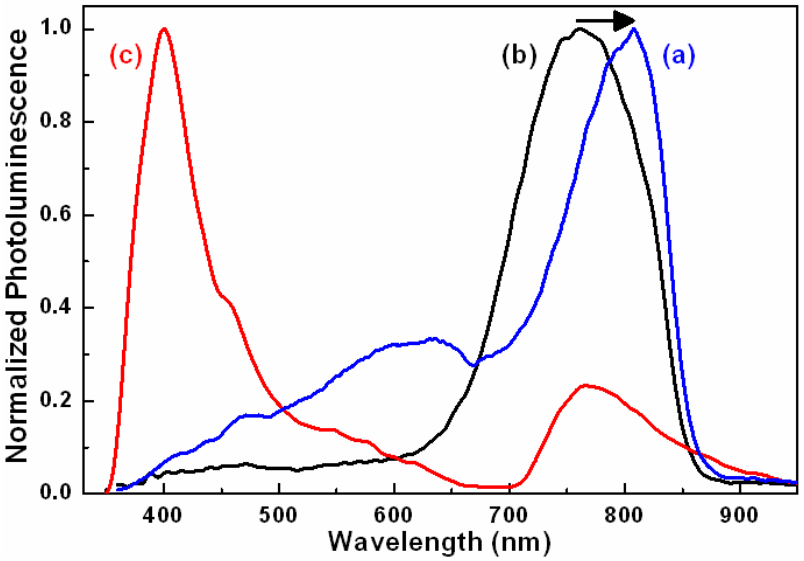

As a result, the simulated $T_{surface}$ of the SiO_x film can be increasing from 130 ^{o}C and 3350 ^{o}C as the CO_2 laser P_{laser} enlarges from 1.5 to 13.5 kW/cm^2. At P_{laser} = 5.8 kW/cm^2 (or $T_{surface}$ = 1285 ^{o}C), the cross-sectional HRTEM image reveals that the diameters of Si nanocrystals precipitated in the SiO_x matrix are ranging from 3 nm to 8 nm, as shown in Fig. 2. The orientation of Si nanocrystals embedded in the SiO_x film is random, including the (111)-orientation with a lattice spacing of about 0.32 nm. The HRTEM estimated density of

the Si nanocrystals in the CO_2 laser RTA SiO_x film at P_{laser} = 5.8 kW/cm^2 is about 4.5×10^{16} cm^{-3}. Similar laser re-crystallization was previously demonstrated by using a tightly focused continuous-wave Ar^+ laser (λ = 514.5 nm), which helps to synthesize Si nanocrystals in the hydrogenated amorphous SiO_x (a-SiO_x:H) film. It was found that the diameter of the Si nanocrystals increases from 2.5 to 12 nm under an extremely high P_{laser} of ranging from 600 kW/cm^2 to 2.6 MW/cm^2. However, the surface damage of the a-SiO_x:H film was also evidenced at such high intensities even with a short irradiating time. A latter experiment showed similar results by using a frequency-tripled Nd:YAG laser at wavelength and pulsewidth of 355 nm and 8 ns, respectively. By increasing the peak energy density of Nd:YAG laser up to 350 mJ/cm^2, the size of Si nanocrystals can be enlarged to 200 nm. Such a process exhibits a similar surface damage problem since the peak P_{laser} of 4.4 MW/cm^2 on the sample surface is far beyond the ablation threshold. Gallas *et al*. then observed that the threshold energy density of a 248 nm-KrF pulsed excimer laser for annealing SiO_x without any ablation is only 85 mJ/cm^2. Nonetheless, only a few Si nanocrystals can be precipitated in SiO_x under such low P_{laser}, since few laser energies are absorbed and transferred to heat by the SiO_x film with infinitely small absorption coefficient of at such short wavelengths (for example, $\alpha < 1\times10^{-6}$ cm^{-1} at <532 nm). In contrast, the CO_2 laser crystallization can precipitate Si nanocrystals at a P_{laser} of at least 2 orders of magnitude smaller than that required for visible or UV lasers, which simultaneously eliminates the laser-ablation induced surface damage effect. The phase separation between Si and oxygen atoms can be initiated when sufficient energy is absorbed by the SiO_x film, however, the annealing temperature for the precipitation of Si nanocrystals should be higher than 900^{o}C. Nesheva *et al*. have observed the formation of amorphous Si nanoparticles in films annealed at 700^{o}C for 1 h. To format the crystallite Si nanocrystals in SiO_x films, a furnace annealing at 1030^{o}C for 1 h is mandatory, as confirmed by Raman scattering analysis. In addition, Yi *et al*. have also demonstrated that the amorphous Si clusters can be formatted at annealing temperature ranging between 300 and 900^{o}C, but the crystallization of these amorphous Si clusters is only observed by annealing in a nitrogen atmosphere at >900^{o}C for 1 h. That is, the annealing temperature of lower than <900^{o}C could not activate the crystallization process for the amorphous Si clusters, even if the annealing duration is lengthened. Under CO_2 laser annealing, the surface temperature of the SiO_x film is dependent on the CO_2 laser intensity, the lower CO_2 laser intensity will reduce the surface temperature of the SiO_x film. Our simulation has also interpreted a threshold annealing

intensity of 4.5 kW/cm^2, which corresponds to a surface temperature of 1100^{o}C for initiating the crystallization of the Si nanocrystals. Similarly, the Si nanocrystals are difficult to be precipitated and the size of the Si nanocrystals could not be larger at a lower CO_2 laser intensity even with longer exposure times.

III-3. CO_2 Laser Ablation Threshold

As the CO_2 laser intensity was larger than the ablation threshold of SiO_x film (6 kW/cm^2), the surface of SiO_x film was sputtered and damaged, which induced oxygen related irradiative defects. The ablation of the SiO_x layer occurs at the CO_2 laser annealing of P_{laser} = 12 kW/cm^2 and leads to another featured PL at 400 nm due to structural damage (see Fig. 1(c)). This results in a concurrent decrease in the near-infrared PL intensity by an order of magnitude, whereas the intensity of blue PL at 400 nm varies oppositely. In fact, the 400-nm PL intensity is increased by one order of magnitude as the P_{laser} increases from 7.5 to 11 kW/cm^2, while the surface temperature has already exceeded the melting temperature of fused silica. Curve-fitting of the broadband PL spectrum from 350 nm to 700 nm reveals three peak wavelengths at 415 nm, 455 nm and 520 nm with associated linewidths of 40 nm, 66 nm and 113 nm as well as the associated irradiative defects of weak-oxygen-bond, neutral oxygen vacancy (NOV) defect and E'$_\delta$ center, respectively.[2-4] Most of these defects are oxygen dependent; and some of them are NOV defects originated from the nc-Si precipitation process as many excessive Si atoms occupied the sites of oxygen move away to precipitate nc-Si. Precipitated nc-Si inevitably compresses the SiO_x matrix and results in the formation of the interstitial oxygen dependent new defects, such as the weak-oxygen bond or ionized oxygen molecule (O_2^-).

The corresponding temperature on the SiO_x surface is up to 1902 ^{o}C as P_{laser} becomes >7.5 kW/cm^2, which has already exceeded over the melting temperature of fused silica. Moreover, a CO_2 laser annealing process at P_{laser} >7.5 kW/cm^2 not only anneals the SiO_x film and precipitates Si nanocrystals locally, but also leads to an increasing of structural damage related PL at 410 nm by at least one order of magnitude. The SiO_x matrix could be promptly compressed during such a rapid laser ablation procedure, where numerous oxygen dependent defects such as weak-oxygen-bond (O-O), oxygen vacancy and ionized oxygen molecule (O_2^-) with PL wavelengths at 410-455 nm are generated by the damaged bonds of the SiO_2 matrix (see the inset (f)-(g) of Fig. 3). Such a phenomenon was never observed in furnace annealed SiO_x film under a similar condition, as the furnace annealing usually causes a gradual recovery on the compressing strain of SiO_2 matrix nearby Si nanocrystals.

III-3. EL of CO_2 Laser Annealed nc-Si LED

The turn-on voltages of ITO/CO_2 laser RTA SiO_x/p-Si/Al and ITO/furnace-annealed SiO_x/p-Si/Al MOSLEDs are 79 and 87 V with slopes of 2.7 and 2.2 (kV/A/cm^2), respectively. Lower turn-on voltage and higher slope of an ITO/CO_2 laser RTA SiO_x/p-Si/Al MOSLED are attributed to the existence of defects buried in CO_2 laser RTA SiO_x film. The electric-field (E) dependent emission current (I) can be described and the current-field plot can thus be fitted by Fowler-Nordheim (FN) tunneling equations listed as below:[13]

$$I_{FN} = A_G A E^2 \exp(\frac{-B}{E}), \tag{2}$$

$$A = \frac{q^3 (m/m_{ox})}{8\pi h \Phi_B} = 1.54\times10^{-6} \frac{(m/m_{ox})}{\Phi_B}\left[\frac{A}{V^2}\right], \tag{3}$$

$$B = \frac{8\pi\sqrt{2m_{ox}\Phi_B^3}}{3qh} = 6.83\times10^7 \sqrt{(m_{ox}/m)\Phi_B^3}\left[\frac{V}{cm}\right], \tag{4}$$

where A_G is the gate area, E is the electric-field, and A and B are usually considered to be constants. m_{ox} is the effective electron mass in the oxide, m is the free electron mass, and Φ_B is the effective barrier height. The FN tunneling behavior can be confirmed, due to the linear transferred function characteristic in the Arrhenius FN plot (see Fig. 2).

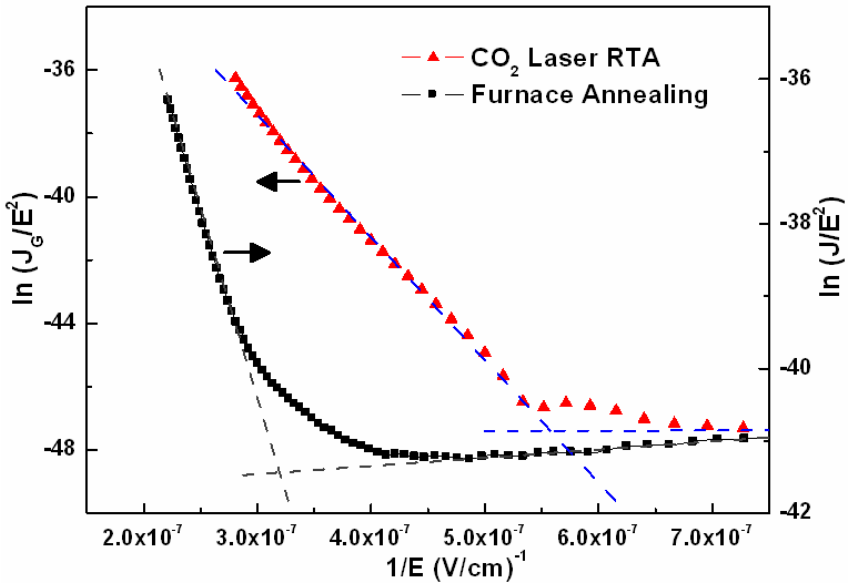

The threshold electric-fields to initiate FN tunneling for CO_2 RTA and furnace-annealed MOSLEDs are 1.8 and 3.2 MV/cm, respectively, which indicates that the effective potential barrier of the sample becomes smaller with the assistance of defects. This essentially corroborates with the reduction on threshold electric-field of FN tunneling occurred in the CO_2 laser RTA sample. The gradient of power-current (P-I) plot of ITO/CO_2 laser RTA

SiO_x/p-Si/Al and ITO/furnace-annealed SiO_x/p-Si/Al MOSLEDs are 33.5 and 17.6 ($\mu W/A/cm^2$), respectively (see Fig. 3). The EL power of the ITO/CO_2 laser RTA SiO_x/p-Si/Al MOSLED with oxygen-related defects can be enlarged by two times as compared to that of the ITO/furnace-annealed SiO_x/p-Si/Al MOSLED with a higher turn-on voltage.

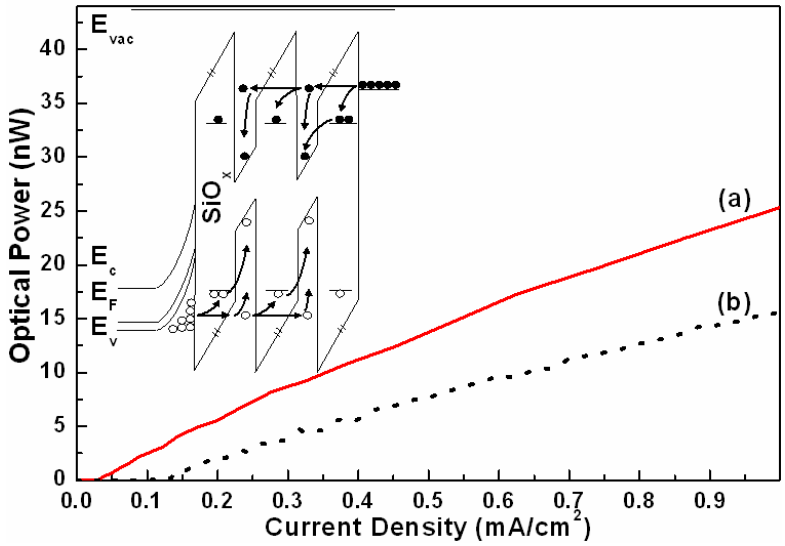

The barrier height of ITO-SiO_x junction is 3.7 eV with electric affinities of 4.7 eV for ITO and 1 eV for SiO_2. The electric affinity and bandgap of Si substrate are 4 eV and 1.12 eV, respectively. Due to the CO_2 rapid-laser-annealing process introduces oxygen-related defects buried in the ITO/CO_2 laser RTA SiO_x/p-Si/Al MOSLED, these oxygen-related defects and interfacial states facilitate the carrier transport into nc-Si for the electron-hole pair recombination (see the inset of Fig. 3), and also decrease the turn-on voltage. This also elucidates the significant reduction of threshold electric-field of the ITO/CO_2-laser-RTA SiO_x/p-Si/Al MOSLED. In contrast to the conventional furnace-annealed MOSLED, the high-temperature and long-term furnace-annealing usually causes a gradual recovery on the compressing strain of the SiO_2 matrix nearby the nc-Si and also contributes a defect-free furnace-annealed SiO_x film, corresponding to the higher turn-on voltage, lower EL power and the difficulty of carrier injection into nc-Si. Consequently, the electrons require a higher electric-filed to tunnel through the barriers of the MOS structure. Furthermore, the enhanced P-I slope and EL power from the CO_2 laser RTA SiO_x based MOSLED are due to the assistance of carrier injection via oxygen-related defects as compared to those of the furnace-annealed SiO_x based MOSLED at same biased condition.

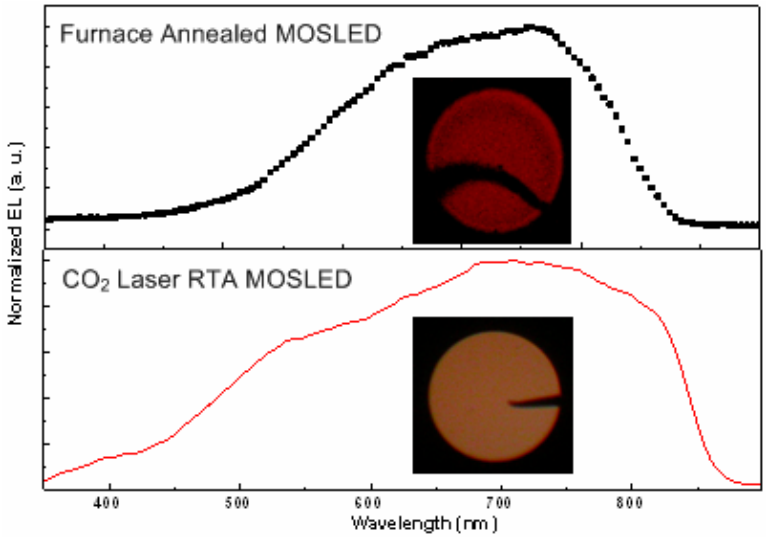

Nc-Si related EL spectra of ITO/CO_2 laser RTA SiO_x/p-Si/Al MOSLED with a bright color far-field pattern was decomposed into three luminescent peaks at 590, 715 and 810 nm with the spectral linewidths of 203, 117 and 54 nm as well as peak ratios of 1.65:1.47:1, respectively (see the lower of Fig. 4). The luminescent peaks at 590 and 810 nm emitting from different size of nc-Si were observed, however, the luminescent peak at 715 nm was not obviously found in the PL spectrum. Because of oxygen-related defects, such as weak-oxygen-bond and NOV defects, behave high energy bandgaps, carriers favor to inject into smaller nc-Si with higher energy bandgaps and approximate excited level via oxygen-related defects, and then recombine in the nc-Si. This result corresponds to the largest decomposed-EL intensity at 590 nm and the reduction of the decomposed-EL intensity as the increasing size of nc-Si. Hence, the EL emission from nc-Si at 715 nm can be enhanced and observed. The EL spectrum of ITO/furnace-annealed SiO_x/p-Si/Al MOSLED, biased at higher electric-field without the carrier-transport assistant of oxygen-related defects, reveals a deep-red far-field pattern (see the upper inset in Fig. 4) and dual luminescent peaks at wavelengths of 625 and 768 nm with spectral linewidths of 189 and 154 nm, respectively. The EL component at longer wavelength coincides well with that of PL, revealing that the nc-Si-related PL and EL are attributed to the same carrier recombination mechanism. The mechanism of secondary EL peak expanded to shorter-wavelength region (500-700 nm) is possibly attributed to the cold-carrier-tunneling process under appropriate bias. Since the band bending becomes serious under an extremely high electric-field, leading to the carriers between adjacent nc-Si tunneled from first-order quantized state (n=1) to second-order quantized state (n=2), providing a higher population in the second-order state as well as an enhanced spontaneous emission at larger energy.

IV. Achievements and Conclusions

In conclusion, the enhanced near-infrared EL of an ITO/CO_2 laser RTA SiO_x/p-Si/Al MOSLED is preliminarily demonstrated. The CO_2 laser RTA performs the *in-situ* and localized temperature control of the SiO_x film, which thus facilitates precipitating Si nanocrystals from damaging the nearby devices. The equivalent temperature of the SiO_x surface is increasing from 130^{o}C to 3350^{o}C as the CO_2 laser P_{laser} enlarges from 1.5 to 13.5 kW/cm^2. Dense nc-Si can be synthesized in the $SiO_{1.25}$ film by using CO_2 laser RTA at P_{laser} of 6 kW/cm^2 for 1 ms. The Si nanocrystals with maximum diameter and density of 8 nm and 4.5×10^{16} cm^{-3}, respectively, can be locally precipitated within the CO_2-laser RTA SiO_x film, giving rise to a near-infrared PL at 790-806 nm. The comparison on PL spectra of CO_2 laser annealed and furnace-annealed PECVD-grown $SiO_{1.25}$ samples reveals the contribution of oxygen related defects. Since the CO_2 laser annealing time is only 1 ms and much shorter than furnace-annealing time (3 hours), the annealing time is insufficient for precipitating larger-size nc-Si, whereas the oxygen-related defects are generated in the CO_2 laser annealed SiO_x film. These are obtained at just below ablation-threshold intensity (6 kW/cm^2), which is at least 2 orders of magnitude smaller than that required for visible or UV lasers. The power dependent μ-PL analysis indicates that the precipitation of small-size Si nanocrystals is initialized when P_{laser} > 4.5 kW/cm^2 and a maximum PL peak wavelength of 825 nm can be observed at P_{laser} = 7.5 kW/cm^2.

Nonetheless, the SiO_x film is ablated with a linear ablation slope of 35 nm/kW/cm^2 at beyond threshold P_{laser} of 6 kW/cm^2. The μ-PR results indicate that the refractive index of the CO_2 laser RTA SiO_x film varies from 1.57 to 1.87 as the P_{laser} increases from 1.5 to 7.5 kW/cm^2. At the P_{laser} < 3 kW/cm^2, the change in refractive index is less than 0.6% since the precipitation of Si nanocrystals has not yet been initiated. The refractive index of SiO_x reaches maximum as the surface temperature increases to 1285^{o}C, while the average diameter of Si nanocrystal is also the largest. Annealing at higher intensities not only damages the SiO_x structure, but also constrains the precipitation and Si nanocrystals and decreases the refractive index of the SiO_x. This eventually degrades the near-infrared PL and reduces the refractive index of the CO_2 laser RTA SiO_x film. These defects enhance the carrier transport through the MOSLED, reducing the tunneling threshold from 3.2 to 1.8 MV/cm as compared to the furnace-annealed sample. The elucidation on the role of the oxygen-related defects played on the improved carrier transport and enhanced light emission properties is

addressed. A maximum EL power of nearly 50 nW from the ITO/CO_2 laser RTA SiO_x/p-Si/Al MOSLED under a biased voltage of 85 V and current density of 2.3 mA/cm^2 is reported to date. With the support from US Air Force, three papers have been accepted to be published in international journals, and several papers were present in top international conferences, including on invited talk, as listed below.

Invited Talks:

[1] Gong-Ru Lin, "Enhanced Electroluminescence from Nanocrystallite Si Based MOSLED by Interfacial Si Nanopyramids", *OSA Topical Conference on Nanophotonics (NANO2007)*, Hangzhou, China, June 18-21, 2007.

[2] Gong-Ru Lin, "White-light and near-infrared electroluminescence of furnace or CO2 laser annealed Si-rich SiO2 with structural defects and Si nanocrystals", *2006 SPIE Symposium on Photonics Europe (PE 2006)*, paper 6195-32, Strasbourg, France, April 3-6, 2006.

[3] Gong-Ru Lin, "Retrospect on the Research of Silicon Nanocrystal Embedded Silicon Oxide Materials and Light-Emitting Devices in NCTU/IEO", *3rd Symposium on Nanophotonics Science and Technology*, Hwalian, Taiwan, September 13-17, 2005.

Journal papers:

[1] Gong-Ru Lin, Chun-Jung Lin, Yu-Lun Chueh, and Li-Jen Chou, "Localized CO_2 Laser Annealing Induced Dehydrogenation/Ablation and Optical Refinement of Si-Rich SiO_x Film with Embedded Si Nanocrystals", *Journal of Nanoscience and Nanotechnology*, Vol. 6, No. 12, pp. 3710-3717, December 2006.

[2] Gong-Ru Lin, C.-J. Lin, L.-J. Chou, and Y.-L. Chueh, "Microphotoluminescence and Microphotoreflectance Analyses of CO_2 Laser Rapid-Thermal-Annealed SiO_x Surface With Buried Si Nanocrystals", *IEEE Transactions on Nanotechnology*, Vol. 5, No. 5, pp. 511-516, September 2006.

[3] Gong-Ru Lin, Chi-Kuan Lin, L.-J. Chou, and Y.-L. Chueh, "Synthesis of Si Nano-Pyramids at SiOx/Si Interface for Enhancing Electroluminescence of Si-Rich SiOx Based MOS Diode", *Applied Physics Letters*, Vol. 89, No. 9, 093126, September 2006. *Selected by Virtual Journal of Nanoscale Science & Technology, Vol. 14, No. 12, September 2006*.

[4] Gong-Ru Lin, Hao-Chung Kuo, Huang-Shen Lin, and Chi-Chiang kao, "Rapid Self-Assembly of Ni Nanodots on Si Substrate covered by a Less-Adhesive and Heat-Accumulated SiO2 Layer", *Applied Physics Letters*, Vol. 89, No. 7, pp. 073108, August 2006. *Selected by Virtual Journal of Nanoscale Science & Technology, Vol. 14,*

No. 9, August 2006.

[5] C.-J. Lin, Y.-L. Chueh, L.-J. Chou, C.-W. Chang, E. W. G. Diau, H.-C. Kuo, and G.-R. Lin, "Countinuous-Wave and Time-Resolved Photoluminescence Analysis of Silicon Nanocrystals Formed by Thermal Annealing of Amorphous Silicon Oxides at Different Times", *Japanese Journal of Applied Physics Pt. 1,* Vol. 45, No. 2A, pp. 1040-1043, February 2006.

[6] Chun-Jung Lin, Chao-Kuei Lee, and Gong-Ru Lin, "Time-resolved photoluminescence analysis of multidose Si-ion-implanted SiO_2", *Journal of Electrochemistry Society*, vol. 153, No. 2, pp. E25-E32, Fabruary 2006. *Selected by Virtual Journal of Ultrafast Science, Vol. 5, No. 1, January 2006.*

[7] Chun-Jung Lin, Gong-Ru Lin, Yu-Lun Chueh, and Li-Jen Chou, "Analysis of Silicon Nanocrystals in Silicon-rich SiO_2 Synthesized by CO_2 Laser Annealing", *Electrochemical and Solid-State Letters*, Vol. 8, No. 12, pp. D43-D45, December 2005.

Conference Papers:

[1] Gong-Ru Lin and Chun-Jung Lin, "Enhancement of Fowler-Nordheim Tunneling Based Light Emission from metal-SiOx-Si MOSLED", the *3rd International Conference on Group IV Photonics*, oral paper FA3, September 13-15, Ottawa Canada, 2006

[2] Gong-Ru Lin and Chun-Jung Lin, "SiOx/Si Interfacial Si Nano-Pyramids Enhancd Electroluminescence from Si-Rich SiOx MOSLED", the *3rd International Conference on Group IV Photonics*, poster paper 22, September 13-15, Ottawa Canada, 2006.

[3] Chun-Jung Lin, Chi-Kuan Lin, and Gong-Ru Lin, "Synthesis of Si Nano-Pyramids at SiO_x/Si Interface for Enhancing Electroluminescence of Si-Rich SiO_x Based MOS Diode", *OSA/IEEE Conference on Laser and Electro-Optics (CLEO2006*), Joint Poster Session I Paper JTuD43, Long Beach, California USA, May 21-26, 2006.

[4] Chun-Jung Lin, Chi-Kuan Lin, Gong-Ru Lin, "Enhanced Electroluminescence of Si-rich SiOx Based MOS Diode by Interfacial Precipitated Si Nano-Pyramids", *2006 Integrated Photonics Research and Applications (IPRA) and Nanophotonics (NANO) Topical Meeting*, Oral paper Nanomaterials NThC5, Uncasville, Connecticut USA, April 24-28, 2006.

[5] Chun-Jung Lin, Gong-Ru Lin, Yu-Lun Chueh, and Li-Jen Chou, "Anomalous Absorption of Silicon Nanocrystals in Silicon-rich $SiO_{1.25}$ Matrix Precipitated by CO_2 Laser Annealing", *2006 Integrated Photonics Research and Applications (IPRA) and Nanophotonics (NANO) Topical Meeting*, Oral paper Nanomaterials NThC4, Uncasville, Connecticut USA, April 24-28, 2006.

[6] Gong-Ru Lin, "White-light and near-infrared electroluminescence of furnace or CO2 laser annealed Si-rich SiO2 with structural defects and Si nanocrystals", *2006 SPIE Symposium on Photonics Europe (PE 2006)*, paper 6195-32, Strasbourg, France, April 3-6, 2006.

[7] Chun-Jung Lin, Hao-Chung Kuo, and Gong-Ru Lin, "Analysis of silicon nanocrystals in silicon-rich SiO2 synthesized by CO2 laser annealing", *2005 Asia-Pacific Optical and Wireless Communications Conference and Exhibition (APOC 2005)*, oral paper 6020-72, Shanghai China, November 6-10, 2005.

V. Acknowledgements

The financial support by Asian Office of Aerospace Research and Development (AOARD), Detachment 2 of the Air Force Office of Scientific Research (AFOSR) under Contract No. FA4869-06-01-0065 AOARD 064071 is also acknowledged.

VI. References

[1] L. Pavesi, L. Dal Negro, C. Mazzoleni, G. Franzo, and F. Priolo, Nature (Lond.) **408**, 440 (2000).

[2] C. J. Lin and G.-R. Lin, IEEE J. Quantum Electronics **41**, 441 (2005).

[3] G.-R. Lin, C. J. Lin, C. K. Lin, L. J. Chou, and Y. L. Chueh, J. Appl. Phys. **97**, 094306 (2005).

[4] G.-R. Lin and C. J. Lin, J. Appl. Phys. **95**, 8482 (2004).

[5] L.-Y. Chen, W.-H. Chen, and F. C.-N. Hong, Appl. Phys. Lett. **86**, 193506 (2005).

[6] M. Perálvarez, C. García, M. López, B. Garrido, J. Barreto, C. Domínguez, and J. A. Rodríguez, Appl. Phys. Lett. **89**, 051112 (2006).

[7] C. Huh, N.-M. Park, J.-H. Shin, K.-H. Kim, T.-Y. Kim, K. S. Cho, and G. Y. Sung, Appl. Phys. Lett. **88**, 131913 (2006).

[8] C. J. Lin, G.-R. Lin, Y. L. Chueh, and L. J. Chou, Electrochem. Solid-State Lett. **8**, D43 (2005).

[9] G.-R. Lin, C. J. Lin, L. J. Chou, and Y. L. Chueh, J. Nanosci. Nanotechnol. **6**, 3710 (2006).

[10] A. Tewary, R. D. Kekatpure, and M. L. Brongersma, Appl. Phys. Lett. **88**, 093114 (2006).

[11] T. R. Shiu, C. P. Grigoropoulos, D. G. Cahill, and R. Greif, J. Appl. Phys. **86**, 1311 (1999).

[12] G.-R. Lin, C. J. Lin, and K. C. Yu, J. Appl. Phys. **96**, 3025 (2004).

[13] R. H. Fowler and L. W. Nordheim, Proc. R. Soc. London, Ser. A119, 173 (1928).